Role for the α-Helix in Aberrant Protein Aggregation†

Rani Kunjithapatham,‡ Fabiana Y. Oliva,‡ Urmi Doshi,‡ Mar Pérez,§ Jesus Ávila,§ and Victor Muñoz*,‡

Department of Chemistry and Biochemistry and Center for Biomolecular Structure and Organization, University of Maryland, College Park, Maryland 20742, and Centro de Biología Molecular Severo Ochoa, Facultad de Ciencias, Universidad Autónoma de Madrid, Cantoblanco, 28049 Madrid, Spain

Received July 7, 2004; Revised Manuscript Received September 27, 2004

ABSTRACT: Is the α-helix structure capable of triggering the formation of aberrant protein aggregates? To answer this question, we investigate the *in vitro* aggregation of tau protein in the presence of the helix-inducing agent TFE. Tau is a natively unfolded protein that binds to microtubules and forms aggregates in Alzheimer's disease. We find that full-length tau has residual α-helix structure, which is further enhanced by three mutations involved in genetic neurological disorders. TFE concentrations matching an α-helical content of 40% in full-length tau and the triple mutant induce the formation of aggregates that are morphologically and structurally heterogeneous. A simple dilution experiment reveals that heterogeneity results from the competition between α-helical fibrillar aggregates and more classical amyloid-like aggregates. The α-helical aggregates are more resilient to dilution and have the spectroscopic features of α-helical coiled coils. We propose a general mechanism by which intrinsically stable α-helices can associate into aggregates with only coarse coiled-coil symmetry. In tau, high intrinsic α-helix stability and coarse coiled-coil symmetry could be byproducts of its biological function.

When Pauling predicted the α-helix and *β*-sheet structures (*1*), he was guided by the molecular symmetry of the two conformations. Molecular symmetry is also at the core of Eisenberg's idea of domain swapping as a general mechanism for protein evolution (*2*). Because of their intrinsic symmetry, α-helices and *β*-sheets are perfect building blocks for supramolecular assembly. α-Helices assemble by formation of coiled coils that then arrange into higher-order fibrillar structures (*3*). Coiled-coil polymers are ubiquitous in biology and provide a variety of structural roles (*3*). There are important examples of *β*-sheet structural polymers, but *β*-sheet polymers are best known in connection with aberrant protein aggregation (*4*). These protein aggregates, which receive the generic name of amyloid fibrils, are associated with the onset of several human diseases (*5*, *6*). A major energetic factor facilitating amyloid assembly is the formation of intermolecular backbone hydrogen bonds. The hydrogen bonding pattern provides a mechanism for symmetric self-propagation that is somewhat independent of the amino acid sequence. Accordingly, aggregation experiments in a variety of proteins suggest that virtually any protein can self-assemble into *β*-sheet-containing fibrils (*6*, *7*).

These observations raise the question of whether aberrant aggregation is an exclusive property of *β*-sheets, or whether there is an additional role for the α-helix. A simple structural argument states that α-helices cannot possibly form aberrant aggregates because they lack the propagation mechanism of *β*-sheets. In α-helical polymers, backbone hydrogen bonds stabilize the α-helix structure, but intermolecular interactions require detailed complementation between side chains. Such intricate networks of side chain interactions should not arise spontaneously, unless specifically selected by natural evolution.

Here we hypothesize that the intrinsic stabilization of α-helix structure can trigger the formation of α-helical aggregates in which the coiled-coil symmetry is only attained at a crude level. To test this hypothesis, we investigate the aggregational properties of tau protein in increasing concentrations of the helix-promoting solvent TFE.[1] TFE stabilizes α-helices nonspecifically by strengthening their hydrogen bonds (*8*). The microtubule-associated protein tau is a natively unfolded protein that aggregates *in vivo* into polymers termed PHFs (*9*). PHFs appear in Alzheimer's disease and in a variety of genetically based neurological disorders (*10*). Recently, we found α-helix structure in *ex vivo* PHFs (*11*), a discovery that was later confirmed using immunopurified PHFs (*12*, *13*). Furthermore, the microtubule binding domain of tau, which constitutes the core of PHFs (*14*), has significant α-helix propensity (*15*) and binds to the C-terminal α−helices of tubulin (*16*, *17*). The presence of α-helix, however, does not imply that formation of PHFs is through helical polymerization. In fact, other groups have reported that PHFs contain *β*-sheet structure, and have proposed a standard amyloid mechanism (*13*, *18*). Because TFE also stabilizes *β*-sheet hydrogen bonds (*19*), our experiments provide a unique opportunity to investigate a putative competition between *β*-sheet- and α-helix-mediated aggregation.

† This work has been funded by the Searle Scholars Program. V.M. is recipient of a Dreyfus New Faculty Award, a Packard Fellowship for Science and Engineering, and a Searle Scholarship.

* To whom correspondence should be addressed. E-mail: vm48@umail.umd.edu. Phone: (301) 405-3165. Fax: (301) 314-0386.

‡ University of Maryland.

§ Universidad Autónoma de Madrid.

[1] Abbreviations: TFE, trifluoroethanol; PHFs, paired helical filaments; SVD, singular-value decomposition; AD, Alzheimer's disease; CD, circular dichroism; AFM, atomic force microscopy; FTIR, Fourier-transformed infrared spectroscopy; ATR, attenuated total reflection.

10.1021/bi048564t CCC: $30.25
Published on Web 12/15/2004

In particular, we are interested in full-length tau (hereafter termed fl-tau). In contrast to many tau fragments, the 441-residue tau isoform is notoriously difficult to polymerize *in vitro* (*20*). Thus, any successful aggregation attempt on this protein has a better chance to be specific, and not just the nonspecific fibrillization so common to structureless peptides (*21*). As a test of biological significance, we also studied a variant of full-length tau that includes three mutations (G272V, P301L, and R406W) which we denote 3m-tau. These three mutations are involved in genetically based dementia disorders, which are characterized by the higher susceptibility of tau to formation of PHFs (*22*).

MATERIALS AND METHODS

Expression and Purification of Wild-Type and Mutant Forms of Full-Length Tau. Clones of full-length human tau inserted in the arabinose-inducible plasmid pRKT42 and mutant G272V/P301L/R406W inserted in the IPTG inducible plasmid pRK172 were expressed as described previously (*23*). The purification protocol followed the one described previously (*23*) with a modification targeted at eliminating the contamination by nucleic acids. The modification consists of increasing the pH of the sample to 12 after the first ammonium sulfate precipitation step (25% w/v) to decrease the net positive charge of tau.

CD Spectroscopy. All the CD spectra were recorded at 298 K in the range of 190−250 nm using a JASCO J-810 spectropolarimeter in continuous scanning mode. The acquisition parameters were 20 nm/min with a 4 s response and a 2 nm bandwidth. TFE titrations were carried out in three steps by stepwise additions of TFE to solutions containing the protein and initial TFE concentrations of 0, 63, and 85%. Protein concentrations were determined colorimetrically using the BCA procedure (Pierce, Rockford, IL). The protein concentration in the initial samples was set to 2.8 μM for fl-tau and to 1.9 μM for 3m-tau, and the samples were prepared in 20 mM phosphate buffer (pH 7). Protein concentrations were redetermined at the end of each of the three dilution runs to check for consistency in the experiment. CD data for both proteins were analyzed by SVD (*24*) to obtain the main components. These components were corrected to mean residue ellipticity units and used to calculate the fraction of each component present in each of the spectra in the series by solving the system of linear equations. To simulate the TFE titrations with the helix−coil algorithm AGADIR (*25*), we performed a series of calculations in which the strength of the mean enthalpic contribution (i.e., hydrogen bond) is progressively increased. The calculations were carried out using the multiple-sequence approximation (*26*) and dividing the 441 residues of tau into 17 overlapping segments of 50 residues. The profile for the whole protein was obtained by selecting for each residue the highest of the two helicity values to eliminate artifacts from the cutting points.

Purification of PHFs (ex vivo). PHFs were purified from brain tissues of AD patients according to the method of Greenberg and Davies (*27*). Samples of AD brain tissue were provided by Dr. Ravid from the Netherlands Brain Bank.

In Vitro Filament Formation. Fl-tau (∼4.5 μM) and 3m-tau (∼4.5 μM) were incubated for 30 days at 310 K in sealed tubes with 20 mM phosphate buffer (pH 7) and 20 and 70% TFE, respectively. The dilution experiment was simply carried out by adding 3 volumes of the incubation buffer to the sample.

Atomic Force Microscopy. AFM samples were prepared by depositing 5 μL of the solution on the mica surface, followed by incubation for 1 min to optimize adsorption. The samples were then washed with 5 mL of water and dried with nitrogen. AFM images of the dried samples were obtained in tapping mode using Super Silicon Sharp probes (SSS-NCH by Nanosensors) with a tip radius of curvature of <5 nm in a Multimode Scanning Probe Microscope from Veeco Instruments Inc. The analysis of the images was carried out with custom-made algorithms written in MATLAB code.

FTIR Spectroscopy of in Vitro-Grown Tau Filaments. FTIR spectra were measured using an Excalibur FTS 3000 spectrometer from MX-BIORAD equipped with a Harrick ConcentratIR horizontal multiple-reflection ATR accessory. For each spectrum, 4096 interferograms at 4 cm^{-1} resolution were co-added and Fourier transformed using triangular/Mertz apodization. Twelve different spectra were measured for each sample and then averaged to minimize artifacts from the heterogeneity of the sample. Spectra were taken in liquid (aqueous solution) and on film by letting the sample dry on the crystal surface. No changes in spectral shape were observed between the liquid and film spectra. The second-derivative analysis and fits to series of Gaussian curves were performed using MATLAB.

RESULTS AND DISCUSSION

Conformational Properties of Tau Proteins. To analyze the helical propensity of the two proteins, we measured the far-UV CD spectrum of ∼2.5 μM samples of each protein at TFE concentrations ranging from 0 to 94% (Figure 1a,b). From the SVD of the combined data, we obtain three main components that correspond to CD spectra of α-helix, random coil, and β-sheet (Figure 1c). The calculation of secondary structure from the three components reveals that the α-helix content of fl-tau increases from ∼15% in water to ∼65% at the highest TFE concentration. 3m-tau has a higher α-helix content in water (∼20%), which increases to almost 90% (Figure 1d). The complexity of the TFE response curves indicates that the distribution of α-helix propensity in these proteins is heterogeneous. It is for this reason that no isodichroic point is observed. In 3m-tau, a small population of β-sheet is also observed (Figure 1d), illustrating that our analysis is sensitive to as little as 2% β-sheet structure. The β-sheet population of 3m-tau peaks at 35% TFE, coinciding with the region in the phase diagram of TFE/water mixtures at which globular proteins exhibit a stronger propensity to aggregate into β-sheets (*28*).

In experiments at higher protein concentrations, we observed an increase in β-sheet content at the expense of the random coil (data not shown), confirming the connection with self-association reactions. The increase in β-sheet content with increasing protein concentrations was clear in 3m-tau, but barely apparent in fl-tau. Presumably, this differential behavior is due to the substitution of three polar residues with hydrophobic residues in the mutant. At protein concentrations of >5 μM, we observed protein precipitation during the titration. Precipitation started at 23% TFE for 3m-tau and at ∼70% for fl-tau. The emergence of precipitation

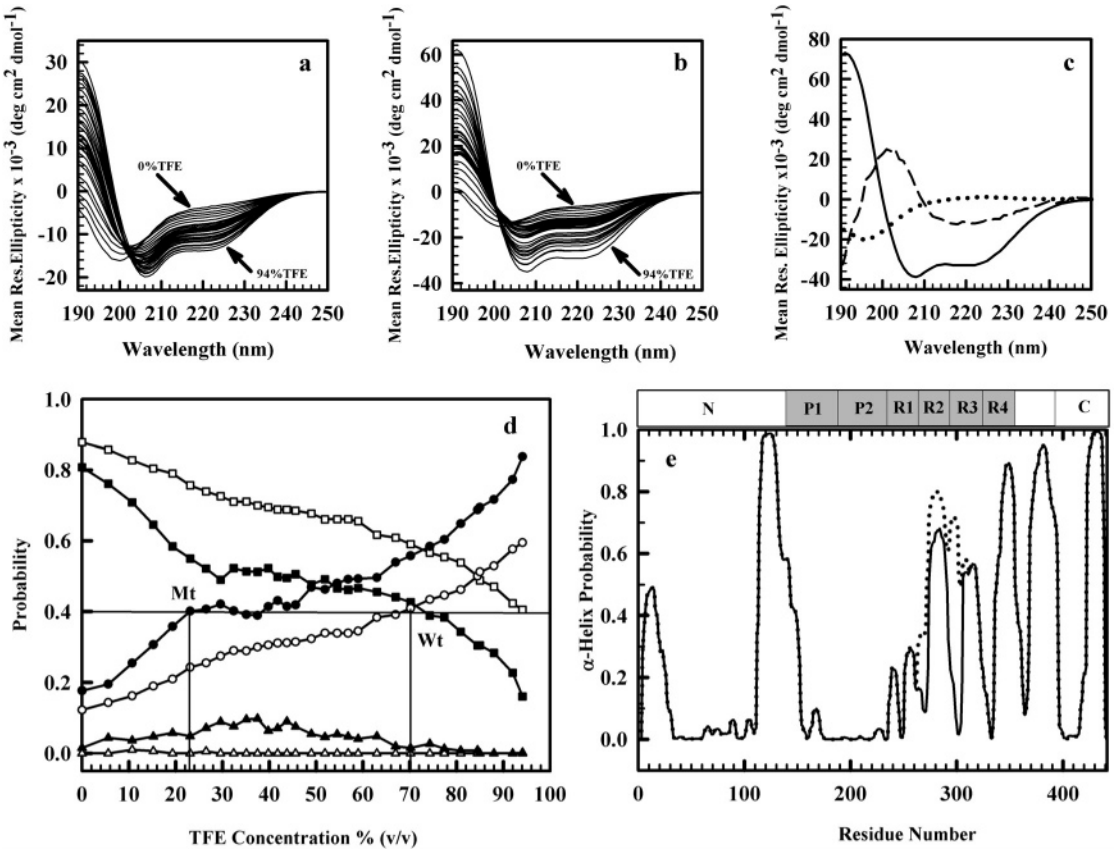

FIGURE 1: Conformational changes in tau induced by TFE. (a) TFE titration of fl-tau. (b) TFE titration of 3m-tau. (c) Spectra of three basic CD components obtained by SVD: α-helix (—), random coil (•••), and β-sheet (− − −). (d) Relative populations of the three components as a function of TFE for fl-tau (open symbols) and 3m-tau (filled symbols), with circles for α-helix, squares for random coil, and triangles for β-sheet. (e) Distribution of α-helix probability at the residue level in TFE concentrations equivalent to an α-helical content of ∼40%, as calculated with AGADIR: (—) fl-tau and (•••) 3m-tau.

does not correlate with the amount of β-sheet present in the sample, but rather with the amount of α-helix. Indeed, these values correspond to TFE concentrations at which each protein achieves ∼40% of the α-helix content (see Figure 1d), providing a first link between aggregation and α-helix formation. To investigate how the 40% α-helical content is distributed throughout the 441 residues of tau, we simulated the TFE titration experiments using the helix−coil algorithm AGADIR (*25*). AGADIR is a statistical mechanical model of the helix−coil transition that incorporates many of the sequence-dependent energetic contributions to α-helix stability. This algorithm has proven to be extremely useful in predicting the α-helical content and the distribution of α-helix propensity along the sequence of a large number of peptides (*25*). The calculation with AGADIR (see Materials and Methods) reveals that the α-helical population is clustered in a few regions of high intrinsic stability (Figure 1e). The regions with high stability correspond to the last three microtubule-binding repeats, the next 30 residues, a region of ∼40 residues in the C-terminal domain, and another ∼40-residue region at the end of the N-terminal domain. Therefore, there is a strong overlap between regions of high helical propensity and the segment of tau that becomes the core of PHFs (*14*). The calculation also indicates that the increase in α-helix content induced by the three mutations of 3m-tau is a consequence of the increase in intrinsic α-helix stability of microtubule-binding repeats 1 and 2.

In Vitro Aggregation of Tau: Morphological and Structural Heterogeneity. In an attempt to induce tau aggregation in a more controlled fashion, we incubated each tau protein at a protein concentration of ∼4 μM and at a TFE concentration slightly below the observed threshold for precipitation. In particular, 3m-tau was incubated in a solution containing 20% TFE and fl-tau in a solution containing 70% TFE. After the mixture had been incubated for 30 days at 310 K, protein aggregates were detected by AFM in samples of the two proteins, regardless of whether they were incubated with or without stirring and/or 100 mM salt. The ultrastructural analysis with AFM shows that the aggregates are heterogeneous in both morphology and size (Figure 2). The various aggregates can be classified into four main groups. There are amorphous clusters (type 1 in Figure 2), short thin twisted fibrils (type 2), long thin fibrils (type 3), and short thick rolled-up fibrils (type 4). Type 2 aggregates only appear at short incubation times and seem to be precursors of type 4 aggregates (see below). This general classification of aggregates applies to all samples, but there are quantitative differences among them. 3m-tau consistently produces more aggregates than fl-tau, and larger amounts of aggregates are found in the absence of stirring and salt. In 3m-tau, type 1 aggregates appear very early in the reaction, and progressively decrease in concentration as the incubation time increases. At the longest incubation times (i.e., >30 days), 3m-tau samples are pervaded of type 3 and 4 aggregates. Fl-tau forms a larger amount of amorphous

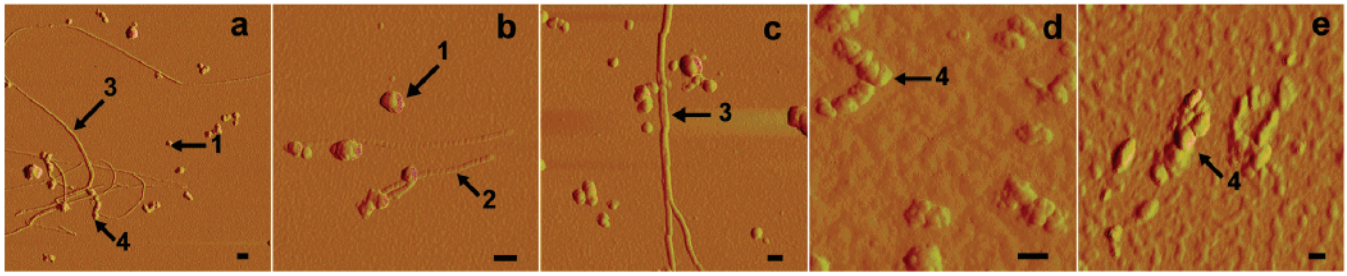

FIGURE 2: Morphological heterogeneity in TFE-aggregated 3m-tau (a−d) and fl-tau (e). (a and b) AFM amplitude images at intermediate incubation times. (c and d) AFM amplitude images at late incubation times. (e) AFM amplitude image of fl-tau sample at late incubation times. The four types of aggregates are highlighted with arrows. The black bar is 100 nm long.

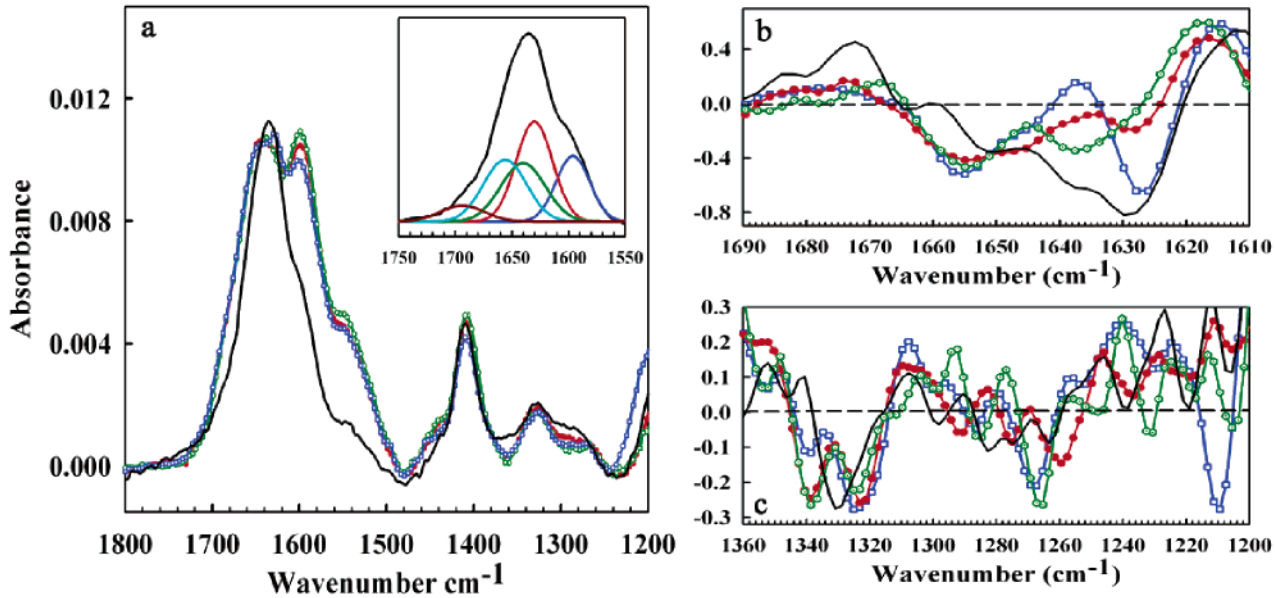

FIGURE 3: FTIR of TFE-aggregated 3m-tau. (a) Intensity-normalized amide I, II, and III bands of 3m-tau in aqueous buffer (green), in 20% TFE (red), in 20% TFE incubated for a long time (blue), and in 20% TFE incubated for a long time and 4-fold diluted (black). The inset shows the amide I band of 3m-tau incubated for a long time and 4-fold diluted corrected for baseline and showing the fit to five Gaussian curves with mean values at 1596, 1630, 1640, 1654, and 1694 cm^{-1}. (b) Second derivative of the amide I band. (c) Second derivative of the amide III band. The color code is maintained throughout.

type I aggregates together with type 4 aggregates that have a less regular appearance (Figure 2e). Type 1 aggregates are still present in fl-tau at the longest incubation times, and no type 3 aggregates could be observed.

To investigate the structural properties of the fibrillar aggregates, we concentrated on the protein and conditions that resulted in a higher level of and more regular fibrillization: 3m-tau incubated for 30 days in 20% TFE and in the absence of salt and stirring. Under these conditions, only 55 ± 5% of the 3m-tau molecules remain in solution after the samples had been spun down at 14 000 rpm for 30 min, indicating that at least 40% of the total protein is involved in some sort of sizable aggregation. Figure 3a shows the amide I, II, and III regions of the FTIR spectrum of this sample. FTIR spectra of 3m-tau in water and in 20% TFE with no incubation are also shown for reference. The amide I and III bands of the three samples are broad and complex, indicating structural heterogeneity. The differences among them are better ascertained in the second derivative of the spectrum (panels b and c of Figure 3 for amide I and III bands, respectively). The amide I band of 3m-tau in water has maxima at 1655 and 1638 cm^{-1}, as expected for a mixture of α-helix and coil. In 20% TFE, the band at 1638 cm^{-1} disappears, and two new bands with maxima at 1647 and 1626 cm^{-1} become observable. In agreement with the CD data of Figure 1, these spectral changes point to a modification in the helical conformations, a decrease in the amount of coil, and the emergence of β-sheet. The spectrum after incubation for 30 days in 20% TFE shows changes in the α-helix signal (1650−1655 cm^{-1}), and a pronounced increase in the sharp β-sheet band at 1626 cm^{-1}. The amide III band also reports about the secondary structure content of polypeptides, but with a larger spectral dispersion: α-helices have frequencies between 1340 and 1300 cm^{-1}, coil conformations range between 1280 and 1240 cm^{-1}, and β-sheets have frequencies below 1240 cm^{-1} (*29*). The second derivative of the amide III band (Figure 3c) supports the conclusions drawn from the analysis of the amide I band.

Isolating α-Helical Aggregates of Tau by Simple Dilution. The morphological heterogeneity of the tau aggregates and the complexity of their FTIR spectrum highlight a problem that might be of general relevance for aggregation studies. Assigning molecular features to the different species present in a heterogeneous mixture is problematic. Reasoning that different aggregates are likely to display a different dependence on protein concentration, we explored the consequences of dilution. This strategy works remarkably well for the TFE-induced aggregates of 3m-tau. A 4-fold dilution of

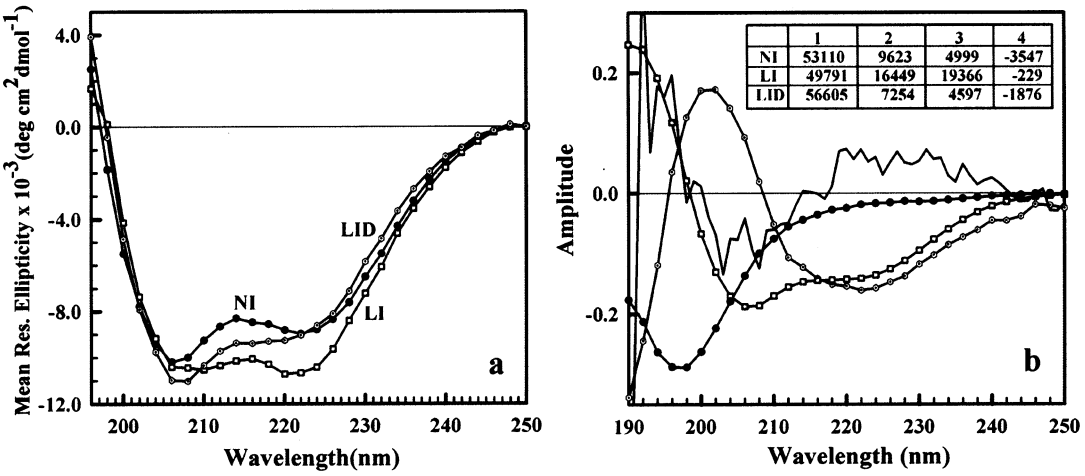

FIGURE 4: CD of TFE-aggregated 3m-tau. (a) Far-UV CD spectrum of 3m-tau in 20% TFE not incubated (NI, ●), incubated for a long time (LI, □), and incubated for a long time diluted 4-fold (LID, ⊙). (b) Four components of the global SVD procedure (in decreasing rank, □, ●, ⊙, and —). The table shows the contribution of each component to each of the spectra in panel a.

3m-tau samples that have been incubated in 20% TFE for more than 30 days results in a structural reorganization that can be followed by CD and FTIR. The structural reorganization takes 2−3 h before reaching a steady state, which remains constant for at least 1 day (data not shown). The morphological analysis by AFM shows that after dilution protein aggregates of type 3 have disappeared. Not a single type 3 fibril could be found in a scanned area of ∼10000 μm^2 of the diluted sample, whereas a similar area of the sample before dilution typically includes more than 100 very long type 3 fibrils. In contrast, the diluted sample has a large number of single type 4 fibrils and agglomerates of type 4 fibrils. The relative amount of nonpelletable protein increases only slightly upon dilution (i.e., 65 ± 5%). Therefore, type 4 aggregates are the largest fraction of aggregated protein in the original 3m-tau sample, and remain largely unperturbed 1 day after diluting the sample 4-fold.

The FTIR spectrum of the incubated, diluted sample of 3m-tau has a sharper amide I band, as expected for a more homogeneous sample (Figure 3a). The second derivative of the amide I region (Figure 3b) highlights three bands with maxima at 1630, 1638, and 1652 cm^{-1}. Fitting of the amide I region to a series of Gaussian curves confirms the presence of three bands at 1630, 1640, and 1654 cm^{-1} with 33, 20, and 21% of the total intensity, respectively (inset of Figure 3a). This pattern of frequencies coincides with the signature FTIR spectrum of the α-helical coiled-coil domains of all intermediate filament proteins (*30*). Application of the Gaussian fitting procedure to the previously published amide I FTIR spectrum of *ex vivo* PHFs (*11*) also produces bands at 1630, 1639, and 1654 cm^{-1}, but in this case with the band at 1654 cm^{-1} having the highest intensity (data not shown). In addition, the β-sheet content present in the long incubated sample of 3m-tau seems to disappear after dilution, as indicated by the absence of the sharp 1626 cm^{-1} peak and the decrease in intensity at frequencies higher than 1660 cm^{-1}. The second derivative of the amide III band (Figure 3c) confirms the absence of β-sheet structure in the diluted sample, and shows the consolidation of a single strong band in the α-helical region (i.e., above 1300 cm^{-1}). Because this FTIR spectrum has been measured by ATR on wet and dry films, it should mainly correspond to the faster depositing aggregated material.

CD, on the other hand, reports on the average structural features of the aggregated-soluble mixture. Far-UV CD spectra of 3m-tau samples incubated for 30 days before and after dilution are shown together with the CD spectrum of a 20% TFE nonincubated sample in Figure 4a. The SVD analysis of these spectra combined with the data of Figure 1 renders four components (Figure 4b). The first component is the average spectrum. As before, the second and third components are random coil and β-sheet spectra, respectively. The noisy fourth component shows an anticorrelation between the α-helix minimum at 208 nm and the other two α-helix extrema at 193 and 222 nm. This component can be assigned to the characteristic length dependence of the α-helix CD spectrum (*31*). From the relative contribution of each component (inset of Figure 4b), we conclude that after incubation for 30 days the β-sheet content has increased 4-fold (from ∼4 to ∼15%). This is accompanied by a smaller increase in the coil, and an increase in the average helix length (more intense minimum at 208 nm). After dilution, the β-sheet and coil contents decrease to the levels before incubation, the contribution of the first component increases, and the average helix length decreases slightly. Taken together, these results suggest that the formation of the β-sheet aggregates requires melting of α-helix structure in the monomer. Upon dilution, the β-sheet aggregates dissolve, and the solubilized molecules regain the α-helix content of the monomeric protein in 20% TFE. The increase in average helix length reflects the consolidation of some of the short and flickering α-helices of the monomer into longer coiled-coil helices in the aggregate. This signal is partially dampened after dilution because the fraction of monomeric α-helices increases.

Morphological Properties of in Vitro Tau Aggregates versus ex Vivo PHFs. Our *in vitro* experiments produce two different kinds of fibrillar aggregates: β-sheet-containing type 3 aggregates and α-helical type 4 aggregates. Type 3 aggregates are only found in experiments with 3m-tau at high protein concentrations, and under those conditions amount to ∼10% of the total protein (vs ∼35% of type 4 aggregates). Furthermore, in contrast with the characteristic resistance to dilution of pathological amyloids, type 3 aggregates quickly disassemble after a 4-fold dilution. All of these observations

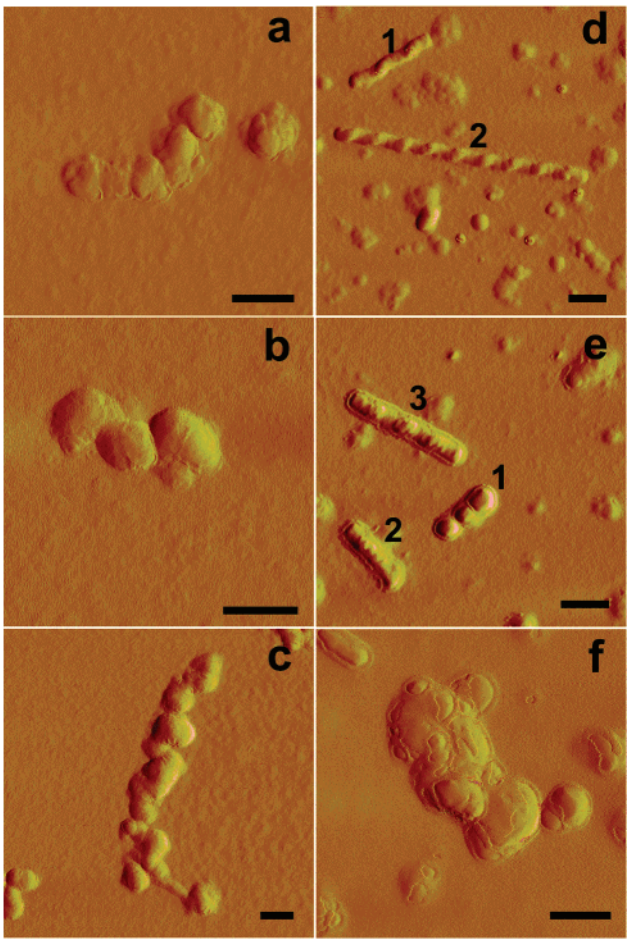

FIGURE 5: AFM amplitude images of type 4 fibrils (a−c) and *ex vivo* PHFs (d−f). The black bar is 100 nm long.

suggest that our type 3 aggregates are nonspecific unstable β-amyloids, and thus unrelated to the formation of PHFs. This idea is further reinforced by the very different dimensions displayed by type 3 aggregates and PHFs. Type 3 aggregates are thin (i.e., ~3.5 nm in height) flat fibrils that bundle up in undetermined numbers, producing fibrillar particles with large variations in width and no apparent periodicity (see Figure 2c for an example). These fibrils are also much longer than typical *ex vivo* PHFs.

α-Helical type 4 aggregates are more resilient to dilution and are formed by both proteins, 3m-tau and fl-tau. This suggests that type 4 aggregates are specific for the tau sequence and, perhaps, more closely connected to the formation of PHFs *in vivo*. In Figures 5 and 6, we compare the morphological properties determined by AFM of type 4 fibrils (panels a−c in Figure 5) and *ex vivo* PHFs (panels d−f). PHFs are often described as twisted ribbons with a periodicity of ~80 nm. PHF d2 (in Figure 5d) is a good representative of such an idealized particle. It is 800 nm long and has nine complete twists with a periodicity of ~78 nm. The height profile (Figure 6c) shows that the peaks have a height of ~12 nm and troughs of ~7 nm. The widths measured by AFM at 80% of the maximal height are ~20 and ~25 nm, respectively (Figure 6d). The broadening on the $x-y$ plane results from a combination of two effects: an image convoluted with the pyramidal shape of the AFM tip and the characteristic "fuzzy coat" of PHFs (*14*). Here we have minimized the influence of the first factor using ultrasharp silicon tips with a characteristic tip radius of ~2 nm. PHFs with such idealized properties are frequently observed, but there also is large variability in their morphology. The shorter PHFs labeled d1 and e3 (Figure 5d,e) have different periodicities (Figure 6b). Other PHFs are mainly flat (5e2) and typically classified as straight filaments, or even appear as rolled-up fibrils (e1). Nevertheless, all these morphologies have height profiles with peaks of ~12 nm and troughs of ~7 nm (Figure 6a,b), in what seems to be their most characteristic ultrastructural property. Sometimes, two PHF particles intertwine with each other (Figure 5f), resulting in a longer pitch and in height profiles with peaks and troughs that are twice as high (Figure 6c).

Although clearly more irregular, α-helical type 4 fibrils have similar general properties. The fibril shown in Figure 5a has a height profile with peaks of ~12 nm and troughs of ~6 nm, and peak-to-peak distances between 60 and 90 nm (Figure 6a). The short fibril 5b has a similar height profile, and a periodicity of ~80 nm (Figure 6b). The much longer fibril 5c has regions that are typical of a single type 4 aggregate, together with regions wrapped around a second type 4 fibril. There is even a region on the bottom of the 5c fibril that has the dimensions and height profile of a type 2 fibril with a periodicity of ~20 nm (Figure 6d). This feature is occasionally observed in the sample, together with short regions with dimensions of two or three wrapped-around type 2 fibrils and periodicities of ~40 or ~60 nm in otherwise typical type 4 fibrils (data not shown), thus suggesting that type 4 fibrils are formed by four type 2 fibrils wrapped around each other.

Type 4 fibrils are frequently bent, while PHFs are straight. But, the most apparent difference between *ex vivo* PHFs and type 4 fibrils is found in the cross section. Type 4 fibrils have significantly larger widths (~33 and ~40 nm for peaks and troughs at 80% of the maximal height) and much more pronounced wings (Figure 6d). Their surface also appears rougher. These differences make the AFM images of type 4 fibrils look quite different from those of PHFs. The coincidence of their height profiles, however, suggests that type 4 fibrils and PHFs may share the same architecture. The rigid core of PHFs only includes a tau segment of ~90 residues, while the remainder of the protein appears as a fuzzy coat under the electron microscope (*14*). As discussed above, the fuzzy coat broadens the $x-y$ plane of the AFM image (particles look wider) but has a minimal effect on the z-axis. Therefore, the larger wings observed in our type 4 aggregates could be the result of particles with the core of PHFs, but a more extensive fuzzy coat. A larger fuzzy coat should be expected because we have assembled type 4 aggregates from full-length tau variants in which the PHF core accounts for only ~22% of the protein. *Ex vivo* PHFs should have a much less dense fuzzy coat because these particles are also comprised of shorter tau isoforms (*32*) and subjected to significant clipping by proteases *in vivo* (*14*).

Structural and Biological Implications. Our results demonstrate that the stimulation of α-helix propensity in tau can trigger the formation of aberrant α-helical aggregates. In analogy to the assembly of biologically functional α-helical polymers, we find that the aggregation process involves the arrangement of preformed α-helices into coiled coils. These findings provide a direct molecular mechanism for α-helical protein fibrillization, which could explain recent reports of

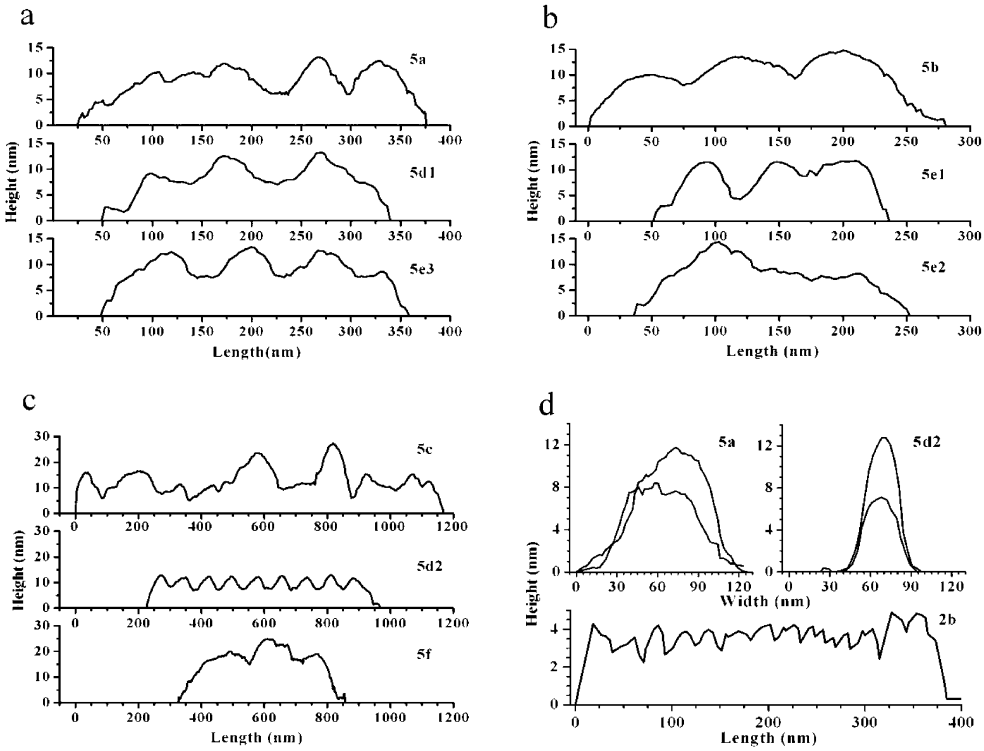

FIGURE 6: Dimensions of type 4 fibrils and *ex vivo* PHFs. (a−c) Height profiles of particles shown in Figure 5. The code name indicates, in order, the figure, panel, and label of the particle. (d) Typical widths of a type 4 fibril (top left) and an *ex vivo* PHF (top right) and height profile of a type 2 fibril (bottom).

tau (*11*−*13*) and ure-2p (*33*) having increased α-helix content in their aberrant aggregated state. By inducing fibrillization of tau with TFE, we also obtain clues about the specificity of the aggregation reaction. TFE also stabilizes *β*-sheets (*19*) and stimulates *β*-amyloid formation (*28*), explaining recent reports of TFE promoting the effect of heparin in inducing the aggregation of tau fragments into *β*-sheet fibrils (*15*). However, in the absence of heparin, TFE favors the assembly of tau into α-helical aggregates that also prove to be more stable. These observations suggest that the formation of tau α-helical aggregates is specific and triggered by structural changes. In contrast, the *β*-sheet aggregates that form under our conditions are nonspecific, and presumably produced by an overall decrease in tau solubility induced by TFE and mutations. Such an effect would be analogous to the changes in the propensity to form *β*-amyloids that have been observed in structureless peptides upon slight variations in hydrophobicity (*21*). A similar mechanism could perhaps explain the *in vitro* amyloidogenic effect that the polyanion heparin has on the positively charged recombinant tau (*13*, *18*).

While the capability of forming amyloids is almost universal given the right experimental conditions, the propensity to assemble into aberrant α-helical aggregates must be a more specific byproduct of biological function. The propensity of tau to aggregate into α-helical coiled coils could arise from its microtubule binding function. The α-helix-prone microtubule binding repeats of tau are likely to bind to the two C-terminal α-helices of tubulin (*17*) by forming heteromolecular coiled coils. It has been long known from *de novo* protein design efforts that the molecular symmetry of heteromolecular coiled coils is compatible with formation of their homomolecular counterparts (*34*). Furthermore, the algorithm COILS (*35*) identifies microtubule binding repeats 1 and 3 of tau as having propensity to become parallel homodimeric coiled coils.

From a structural standpoint, the ability of α-helices to form aberrant aggregates is another manifestation of the importance of molecular symmetry in structural biology. But what biological factors could stabilize the α-helix structure of tau, triggering the formation of helical aggregates? An obvious possibility is the presence of mutations. Here we have shown that the mutations of 3m-tau, which are associated with neurological disorders and increased susceptibility to form PHFs in neurons (*22*), increase the α-helix propensity of tau and promote its aggregation into α-helical aggregates.

Phosphorylation of tau could be an important nongenetic factor. Tau molecules present in PHFs are hyperphosphorylated at sites flanking the microtubule binding domain (*36*). It is well-documented that phosphorylation of serine and threonine enhances their ability to initiate α-helix formation (*37*). Furthermore, phosphorylation can counterbalance the excess of positive charges, and increase the rigidity of the central segment of tau by enhancing its polyelectrolyte character (*38*). Both effects should facilitate the formation of the coiled coils, producing regular straight polymers that are more like *ex vivo* PHFs. Interestingly, naturally phosphorylated bovine tau spontaneously forms ∼2 nm wide filaments that are similar to α-keratin protofibrils (*39*). Our type 2 precursor fibrils have dimensions compatible with two of these ∼2 nm tau filaments wrapped around each other with a periodicity of ∼20 nm. It is also conceivable that microtubules act as heteromolecular templates for the aggregation of tau into coiled coils. This notion is supported by recent findings that tau intercalates between tubulin dimers when present during microtubule polymerization, and also

binds more loosely to the surface of preformed microtubules (*40*). All of these factors indicate that tau has the potential to form α-helical aggregates *in vivo* and independent of amyloid formation. Future studies targeted at investigating some of these factors should further clarify the interplay among the α-helix, the β-sheet, and the formation of PHFs by tau.

ACKNOWLEDGMENT

We are indebted to Mourad Sadqi for help in preparing the figures and to George Lorimer and Eva de Alba for comments on the manuscript.

REFERENCES

1. Pauling, L., and Corey, R. B. (1951) Configuration of Polypeptide Chains, *Nature 168*, 550−551.
2. Bennett, M. J., Choe, S., and Eisenberg, D. (1994) Domain Swapping: Entangling Alliances between Proteins, *Proc. Natl. Acad. Sci. U.S.A. 91*, 3127−3131.
3. Parry, D. A. D., and Steinert, P. M. (1999) Intermediate filaments: Molecular architecture, assembly, dynamics and polymorphism, *Q. Rev. Biophys. 32*, 99−187.
4. Sunde, M., Serpell, L. C., Bartlam, M., Fraser, P., Pepys, C., and Blake, C. C. (1997) Common core structure of amyloid fibrils by synchrotron X-ray diffraction, *J. Mol. Biol. 273*, 729−739.
5. Sunde, M., and Blake, C. C. (1998) From the globular to the fibrous state: Protein structure and structural conversion in amyloid formation, *Q. Rev. Biophys. 31*, 1039.
6. Dobson, C. M. (2003) Protein folding and misfolding, *Nature 426*, 884−890.
7. Fandrich, M., Fletcher, M. A., and Dobson, C. M. (2001) Amyloid fibrils from muscle myoglobin, *Nature 410*, 165−166.
8. Luo, P. Z., and Baldwin, R. L. (1997) Mechanism of helix induction by trifluoroethanol: A framework for extrapolating the helix-forming properties of peptides from trifluoroethanol/water mixtures back to water, *Biochemistry 36*, 8413−8421.
9. Kidd, M. (1963) Paired helical filaments in electron microscopy of Alzheimer's disease, *Nature 197*, 192−193.
10. Yancopoulou, D., and Spillantini, M. G. (2003) Tau protein in familial and sporadic diseases, *Neuromol. Med. 4*, 37−48.
11. Sadqi, M., Hernandez, F., Pan, U. M., Perez, M., Schaeberle, M. D., Avila, J., and Muñoz, V. (2002) α-Helix structure in Alzheimer's disease aggregates of tau protein, *Biochemistry 41*, 7150−7155.
12. Goux, W. J. (2002) The conformations of filamentous and soluble tau associated with Alzheimer paired helical filaments, *Biochemistry 41*, 13798−13806.
13. Barghorn, S., Davies, P., and Mandelkow, E. (2004) Tau paired helical filaments from Alzheimer's disease brain and assembled in vitro are based on β-structure in the core domain, *Biochemistry 43*, 1694−1703.
14. Wischik, C. M., Novak, M., Edwards, P. C., Klug, A., Tichelaar, W., and Crowther, R. A. (1988) Structural characterization of the core of the paired helical filament of Alzheimer disease, *Proc. Natl. Acad. Sci. U.S.A. 85*, 4884−4888.
15. Hiraoka, S., Yao, T. M., Minoura, K., Tomoo, K., Sumida, M., Taniguchi, T., and Ishida, T. (2004) Conformational transition state is responsible for assembly of microtubule-binding domain of tau protein, *Biochem. Biophys. Res. Commun. 315*, 659−663.
16. Serrano, L., Degarcini, E. M., Hernandez, M. A., and Avila, J. (1985) Localization of the Tubulin Binding-Site for Tau-Protein, *Eur. J. Biochem. 153*, 595−600.
17. Nogales, E., Wolf, S. G., and Downing, K. H. (1998) Structure of the αβ tubulin dimer by electron crystallography, *Nature 393*, 191.
18. Berriman, J., Serpell, L. C., Oberg, K. A., Fink, A. L., Goedert, M., and Crowther, R. A. (2003) Tau filaments from human brain and from in vitro assembly of recombinant protein show cross-β structure, *Proc. Natl. Acad. Sci. U.S.A. 100*, 9034−9038.
19. Blanco, F. J., Jimenez, M. A., Pineda, A., Rico, M., Santoro, J., and Nieto, J. L. (1994) NMR Solution Structure of the Isolated N-Terminal Fragment of Protein-G B-1 Domain: Evidence of Trifluoroethanol Induced Native-Like β-Hairpin Formation, *Biochemistry 33*, 6004−6014.
20. Gamblin, T. C., Berry, R. W., and Binder, L. I. (2003) Modeling Tau polymerization in vitro: A review and synthesis, *Biochemistry 42*, 15009−15017.
21. de la Paz, M. L., and Serrano, L. (2004) Sequence determinants of amyloid fibril formation, *Proc. Natl. Acad. Sci. U.S.A. 101*, 87−92.
22. Spillantini, M. G., Murrell, J. R., Goedert, M., Farlow, M. R., Klug, A., and Ghetti, B. (1998) Mutation in the tau gene in familial multiple system tauopathy with presenile dementia, *Proc. Natl. Acad. Sci. U.S.A. 95*, 7737−7741.
23. Perez, M., Lim, F., Arrasate, M., and Avila, J. (2000) The FTDP-17-linked mutation R406W abolishes the interaction of phosphorylated tau with microtubules, *J. Neurochem. 74*, 2583−2589.
24. Henry, E. R., and Hofrichter, J. (1992) Singular value decomposition: Application to analysis of experimental data, *Methods Enzymol. 210*, 129−192.
25. Muñoz, V., and Serrano, L. (1994) Elucidating the folding problem of helical peptides using empirical parameters, *Nat. Struct. Biol. 1*, 399−409.
26. Muñoz, V., and Serrano, L. (1997) Development of the multiple sequence approximation within the AGADIR model of α-helix formation: Comparison with Zimm-Bragg and Lifson-Roig formalisms, *Biopolymers 41*, 495−509.
27. Greenberg, S. G., and Davies, P. (1990) A preparation of Alzheimer paired helical filaments that displays distinct tau proteins by polyacrylamide gel electrophoresis, *Proc. Natl. Acad. Sci. U.S.A. 87*, 5827−5831.
28. Chiti, F., Webster, P., Taddei, N., Clark, A., Stefani, M., Ramponi, G., and Dobson, C. M. (1999) Designing conditions for in vitro formation of amyloid protofilaments and fibrils, *Proc. Natl. Acad. Sci. U.S.A. 96*, 3590−3594.
29. Singh, B. R. (2000) in *ACS Symposium Series*, American Chemical Society, Washington, DC.
30. Heimburg, T., Schuenemann, J., Weber, K., and Geisler, N. (1996) Specific recognition of coiled coils by infrared spectroscopy: Analysis of the three structural domains of type III intermediate filament proteins, *Biochemistry 35*, 1375−1382.
31. Chen, Y.-H., Yang, J. T., and Chau, K. H. (1974) Determination of the helix and β form of proteins in aqueous solution by circular dichroism, *Biochemistry 13*, 3350−3359.
32. Goedert, M., Spillantini, M. G., Jakes, R., Rutherford, D., and Crowther, R. A. (1989) Multiple isoforms of human microtubule-associated protein tau: Sequences and localization in neurofibrillary tangles of Alzheimer's disease, *Neuron 3*, 519−526.
33. Bousset, L., Briki, F., Doucet, J., and Melki, R. (2003) The native-like conformation of Ure2p in fibrils assembled under physiologically relevant conditions switches to an amyloid-like conformation upon heat-treatment of the fibrils, *J. Struct. Biol. 141*, 132−142.
34. Oshea, E. K., Lumb, K. J., and Kim, P. S. (1993) Peptide Velcro: Design of a Heterodimeric Coiled-Coil, *Curr. Biol. 3*, 658−667.
35. Lupas, A., Vandyke, M., and Stock, J. (1991) Predicting Coiled Coils from Protein Sequences, *Science 252*, 1162−1164.
36. Friedhof, P., von Bergen, M., Mandelkow, E. M., and Mandelkow, E. (2000) Structure of tau protein and assembly into paired helical filaments, *Biochim. Biophys. Acta 1502*, 122−132.
37. Andrew, C. D., Warwicker, J., Jones, G. R., and Doig, A. J. (2002) Effect of phosphorylation on α-helix stability as a function of position, *Biochemistry 41*, 1897−1905.
38. Ha, B. Y., and Thirumalai, D. (2003) Bending rigidity of stiff polyelectrolyte chains: A single chain and a bundle of multichains, *Macromolecules 36*, 9658−9666.
39. Ruben, G. C., Iqbal, K., Grundkeiqbal, I., Wisniewski, H. M., Ciardelli, T. L., and Johnson, J. E. (1991) The Microtubule-Associated Protein Tau Forms a Triple-Stranded Left-Hand Helical Polymer, *J. Biol. Chem. 266*, 22019−22027.
40. Makrides, V., Massie, M. R., Feinstein, S. C., and Lew, J. (2004) Evidence for two distinct binding sites for tau on microtubules, *Proc. Natl. Acad. Sci. U.S.A. 101*, 6746−6751.

BI048564T